Computational Fluid Dynamics study of a corrugated hollow cone for enhanced dew yield

Daniel Beysens, Robert Cooke, Enrico Crobu, Laurent Royon

Computational Fluid Dynamics study of a corrugated hollow cone for enhanced dew yield

Daniel Beysens[1,2], Robert Cooke [3], Enrico Crobu [3], Laurent Royon[4]

[1] Physique et Mécanique des Milieux Hétérogènes, CNRS, ESPCI Paris - PSL University, Sorbonne Université, Sorbonne Paris Cité, 75005, Paris, France

[2] OPUR, 2 rue Verderet, 75016 Paris, France

[3] BuroHappold Engineering, 230 Lower Bristol Rd, Bath BA2 3DQ (United Kingdom)

[4] Université de Paris, LIED, UMR 8236 CNRS, 75013 Paris, France

Abstract

Dew condensation is the result of cooling by radiative deficit between a substrate and the atmosphere. Dew yield can be enhanced in hollow structures like hollow cones where the influence of wind is lowered. Corrugation increases the local tilt angle with horizontal and makes dew drop grow faster on edges, then drops detach sooner and act as natural wipers. However, corrugation increases the heat exchange with surrounding local air, which may reduce cooling.

In order to evaluate these effects on cooling and dew yield, a corrugated, W-shaped hollow cone is compared to the same, smooth structure (S-cone) by Computational Fluid Dynamics. Two softwares were used: Ansys CFX for a pre-study concerning detailed aerodynamics where the computational domain is modeled to obtain a fully developed wind profile assuming an unobstructed inlet and COMSOL Multiphysics for aerodynamics coupled with heat flux, including radiative exchange surface-to-sky and surface-to-surface. Local temperatures can be obtained, which can be related to the dew yield. Turbulence is seen at all speeds but stagnation of the flow is also observed, which limits the convective heat exchanges and facilitates dew formation. At low wind speed, convective heat

exchange is similar for both smooth and corrugated surfaces, and corrugation increases cooling. At higher air flow velocities, convective heat exchange is larger for the W-cone but cooling is only slightly smaller than found on the S-cone. Corrugated W-cone should thus give larger yield than the corresponding smooth S-cone.

Keywords

Water Harvesting; Dew condensation; CFD simulation; hollow cone; corrugated hollow cone

Highlights

- Air flow and surface temperature of smooth and corrugated hollow cones are compared by CFD
- Corrugations enhance dew collection by slope and edge effects
- Corrugations only marginally increases heat losses

1. Introduction and background

In the hydrological cycle, natural dew has the same origin as fog and rain precipitations, namely condensation of the water vapor contained in the atmosphere. The latter results from water evaporated from sea, river, lakes, vegetation and soil. Recent isotopic studies (Kaseke et al., 2017) indeed show that fog and dew have multiple origins and that groundwater in drylands can be recycled via evapotranspiration and redistributed to the upper soil profile as non-rainfall water.

In contrast to precipitations, which condense in the cold regions of the atmosphere, dew, alike radiative fog, forms under radiation cooling of a substrate. Dew water is thus a surface phenomenon, in contrast to precipitations which is a volume process.Natural dew is a common and sometimes significant water source in many ecosystems, especially those in arid and semi-arid areas of the world (see e.g. Monteith, 1963; Baier, 1966; Malek et al., 1999; Agam and Berliner, 2006; Liu et al., 2020). Dew as a source of water for humans has been long ignored, although it is generally a water of good quality (Kaseke and Wang, 2018). Since the last 20 years, many studies aimed to increase the dew

yield up to its theoretical limit on order of $1L/m^2$ (see e.g. the reviews by Tomaszkiewicz et al. (2015) and Beysens (2018)). The dew yield essentially depends on the balance between the surface and atmosphere emissions. Dew yield is limited by the available cooling energy, on order of 60 $W.m^{-2}$ in the humid air conditions where dew can form (Bliss, 1961; Beysens, 2018), the latent heat of condensation and the convective heat flux between the substrate and the surrounding air. The latter increases with wind speed but can be greatly reduced in hollow structures like hollow cones.

Increasing the dew yield needs to augment the cooling energy but also the efficiency of water drops collection. The latter involves the efficiency of droplets shedding by gravity. The effect of gravity increases with the angle of the structure with horizontal; however, radiative cooling diminishes with this angle. A good compromise is a tilt angle of 30° with horizontal (Beysens et al., 2013). Hollow cones with 60° half-angle have thus provided good results for dew condensation and dew collection in outdoor conditions (Clus et al., 2009).

Dew drop collection efficiency can be enhanced by the effect of convex edges where drops grow faster thanks to a solid angle of vapor collection larger than in the middle of the substrate (Medici et al., 2014). Edge drops reaches the critical size where the gravity force overcomes the pinning force sooner and slide down, incorporating the drops on their pathway, acting thus as efficient natural wipers. In addition, corrugation increases the local tilt angle with horizontal (Beysens, 2018), thus increasing locally the gravity forces acting on the drops (Fig. 1). Origami structures that partially combine the above positive effects on dew yield (partly hollow structures, edge effects) have been seen to increase the yield by a factor as large as 400% for small yields (Beysens et al., 2013).

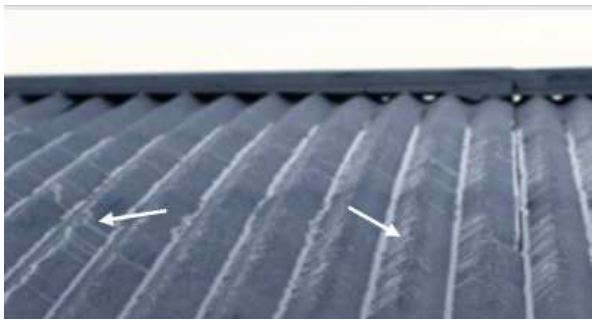

Fig. 1. Drops sliding from the top of corrugations (arrows) on a galvanized iron roof with small tilt angle (≈ 15°). (Combarbala, Chile; Photo J.-G. Minonzio).

Corrugation, however, increases the convective heat exchange with surrounding air and in this aspect may substantially reduce the substrate cooling. In order to estimate the effect of corrugation on a hollow cone, one reports in the following the comparison by Computational Fluid Dynamics (CFD) of a corrugated, W-shaped hollow cone with the same smooth structure, both showing condensing surfaces with nearly 30° angle with horizontal (cone half-angle of nearly 60°). Two softwares were used: Ansys CFX for detailed aerodynamics where the computational domain is modeled to obtain a fully developed wind profile and COMSOL Multiphysics aiming to detail the heat fluxes, including radiative exchange surface-to-sky and surface-to-surface. Since neither Ansys CFX nor COMSOL simulation models include dew formation, an evaluation of dew yield was performed by calculating with COMSOL the local temperatures, which can be related to the dew yield per surface area within some assumptions that will be discussed.

The Ansys CFX was utilised to analyse the proposed design of the cones and test the aerodynamic effects on the airflow velocity over the inner surfaces of the condenser. The metrics used for the aerodynamic performance assessment were based on minimising the air speed as well as maintaining uniform levels of air velocity on the condensing surface. The CFD analysis allowed the cones schema to be optimized by testing various architectural solutions, which resulted into the improvement of the design's aerodynamic performance. A total of five cases were studied from which two candidates were finally selected (Fig. 2). The thermal effects were studied by COMSOL on the two finalists, W- and S-cones.

2. Methods

2.1. The cones

In the pre-study by CFX simulation the cone dimensions are 7.25 m (S-cone upper radius), 5.5 m (W-cone upper radius) with upper part at 10 m above the ground (Fig. 2). The reason for the upper radius difference between S- and W-cones is due to the structural and architectural design of the cones. As the angles of the cones are the same and the height also the same, then the mouth of the S-cone is wider (the W-cone turns up at the edges to create a uniform top edge). The condensing surface area in the W cone is S_{cw} = 100.9m^2, while the one in the S cone is S_{cs} = 187.3m^2. The fact that the W-cone has smaller surface area is due to the fact that the W-cone is inscribed in the S-cone surface, the S cone having a larger diameter than the W-cone.

The COMSOL simulation uses a schematic representation of both W- and S cones where the supporting column has been omitted and the external shape has been schematized (see Fig. 6 below). The goal is indeed to look only to the useful hydrodynamics around the cone and focusing on the air flows and heat exchange inside the funnels. The dimensions of the cones are made identical to better compare their thermal characteristics. The cone dimensions are (S cone) 4.735 m radius and (W cone) 4.635 external radius and 3.944 m internal radius, with both 0.21 m lower radius at 2.554 m below the top. The S-cone half-angle is 60.5° and the W-cone is inscribed in two cones with half-angles 60.0° and 55.6°. The upper part is at 8 m above the ground (Fig. 2). The condensing surface area in the W cone is S_{cw} = 66.8 m^2, while the one in the S cone is S_{cs} = 80.8 m^2. As for the CFX simulation, the W-cone exhibits a smaller surface area because it has a smaller external radius than the S-cone.

Air temperature is set at 15°C and wind speed is varied by steps from 0.5 to 5m/s (CFX) or at two typical values, 10^{-4} and 2 m/s (COMSOL). The CFX simulation deals with the exact shape of the W-cone.

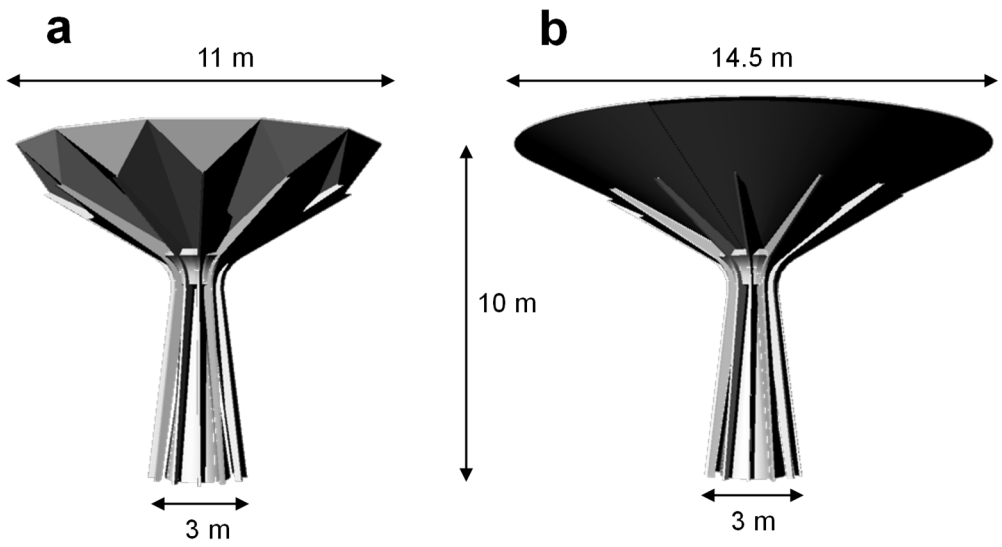

Fig. 2. Geometry of the W-cone (a) and S-cone (b) in the CFX simulation.

2.2. Ansys CFX simulation

As already noted, the Ansys CFX code version 18 is utilised to analyse the proposed design of the cones and test the aerodynamic effects on the airflow velocity over the inner surfaces of the condenser. $k-\varepsilon$ turbulence model is used to simulate mean flow characteristics for turbulent flow conditions. In order to capture the aerodynamic effect of the installation, the geometry includes the lower stand (trunk of the tree) and all the details of the supporting structure that could affect the airflow in the main areas of interest.

The computational size of the domain was developed in line with the recommendations for the assessment of wind conditions around buildings (Mochida et al, 2006). The inlet, the sides and the upper boundary were set at 5 times the cone height H whilst the outflow boundary was set at 15H behind the cone ensuring an appropriate development of the wakes produced by the interaction of the flow with the geometry itself. Unobstructed upstream conditions were also considered as the most likely scenario to take place on site where the condensing trees will be installed.

As summarised by Blocken et al. (2006), the following requirements were implemented:

(i) Sufficient height mesh resolution in the vertical direction in order to allow the height of the first cell to be smaller than 1m

(ii) Horizontal homogeneous atmospheric boundary layer flow in upstream and downstream regions

(iii) Ensuring that the distance between the centre of the first mesh cell and the ground, z_P, is smaller than the height of the terrain physical roughness z_c.

Due to the symmetrical design of the condensing trees, a rectangular computational domain was created for this analysis.

The specification of the atmospheric boundary layer profile is crucial for a correct simulation of the airflow environment. The boundary layer is described as the lower portion of the atmosphere where the wind is largely affected by friction with the surface of the earth. This friction generates turbulence and depends on the type of terrain and geometrical obstructions on the surface. The CFD model used a semi-empirical logarithmic function (see e.g. Pal Arya, 1988) to describe the wind profile $V(z)$:

$$V(z) = V_{10} \frac{\ln\left(\frac{z}{z_c}\right)}{\ln\left(\frac{10}{z_c}\right)} \quad (1)$$

where z_c is the roughness length (taken to be z_c = 0.1 m) and $V_{10}$is wind speed at 10 m off the ground. The logarithmic profile is normally used as inlet condition. The region near to the ground of the domain required special attention as this area is where the interaction between flow and walls happens. If this area of contact is not appropriately defined imprecisions may arise in the CFD assessment. To eliminate this risk a fine mesh was applied to the ground with an inflation layer of 3 steps, whilst the "wall function" was automatically assigned when the $k - \varepsilon$ model was selected.

Side walls and upper domain were modelled using symmetry boundary conditions, whilst a zero-static pressure boundary condition was applied to the outlet. The three-dimensional, steady Reynolds-averaged Navier-Stokes (RANS) equations was solved to simulate the wind flows within the domain. Turbulence was modelled with the $k - \varepsilon$ model as mentioned above.

The computational domain was discretised with a tetrahedral mesh of 6 million cells. An inflation layer of 3 steps, where the first layer's height measured at 0.25m, ensured the adequate mesh resolution at ground level. Several mesh sensitivity tests were carried out. No relevant differences have been identified in the velocity fields of the upstream and downstream flows.

Because of the shape of the faceted crown, the W-cone is expected to produce local acceleration of the flow and accentuated deflection of the flow streamlines. The S-cone instead has a smoother external surface, therefore this shape is expected to reduce flow disruption and facilitate flow acceleration away from the crown.

2.3. COMSOL Multiphysics simulation

The commercial software, COMSOL Multiphysics, was used to analyze the heat transfer and fluid flow taking place around the cones, also using the $k-\varepsilon$ turbulence model to simulate the mean flow characteristics for turbulent flow conditions. The goal of this modeling effort is to predict the temperature of the condenser surfaces for different values of air velocity. In the fluid domains, the continuity equations as well the Navier-Stokes and the energy conservation equations have to be solved simultaneously.

The cones structure is made of Styrofoam to ensure thermal isolation. The simulation of the dew condenser heat exchange takes in account the following processes:

(i) Thermal behavior of the radiative material and the insulation material, including its thermal conductivity, thermal expansion, density, heat capacity and emissivity in the atmospheric window whenever known (see Table 1). For simplicity, the radiative and insulation materials have been taken the same (Styrofoam).

(ii) Radiative cooling power, which depends on the condenser geometry and also on atmospheric conditions (condenser and sky emissivity, air temperature T_a, cloud cover N).

(iii) Incoming diffusive and convective (free or forced) heat exchange with air, which depends on wind speed V, wind speed direction and condenser geometry. The condensation process is not accounted for in the model ("dry air" approximation). The equations of momentum, continuity and temperature are solved by using the numerical code.

In the simulation only typical night conditions are considered, e.g. clear sky N=0, T_a = 288.15 K (15°C), relative humidity RH = 80%. These conditions correspond to a dew point temperature T_d =

11.8°C. Standard numerical values are used for the air properties (density, thermal conductivity, specific heat, etc., see Table 1). Emissivities are taken in the atmospheric window. The most interesting result of the simulation is the local temperature of the condenser, from which the dew yield can be deduced (see Appendix 1).

	$k\ (Wm^{-1}K^{-1})$	$\nu\ (m^2.s^{-1})$	$C_p\ (J\,kg^{-1}K^{-1})$	$\rho\ (kg\,m^{-3})$	$\alpha\ (10^{-3}\,K^{-1})$	ε
Air (15°C)	0.026	$2.2\ 10^{-6}$	1006	1.17	3.4	0.80[a]
Styrofoam	0.035	$8.9\ 10^{-7}$	1300	30	0.20	0.60[b]

Table 1. Some thermophysical properties of air and condenser. k: Thermal conductivity. ν: kinematic viscosity. C_p: Specific heat; ρ: density; α: volumic thermal expansion coefficient; ε: emissivity, hemisphere integrated, wavelength window. (a): Average for atmosphere, see Beysens (2018). (b) 5µm wavelength.

Boundary conditions for air velocity are the same as with CFX, namely air velocity follows the classical logarithmic variation with respect to elevation z according to Eq. (1), with $z_c = 0.1$ m:

(ii) "No-slip" conditions on condenser surfaces and ground.

(iii) "Open frontier" on ceiling and the two vertical sides of the fluid domain.

(iv) "Convective flow" at the exit.

Heat transfer from the air to the surface of the condenser occurs by forced convection. The complete energy equation has thus to be solved in the fluid domain using the velocities found from the solutions of the continuity equation and conservation of momentum equation (Navier-Stokes). The energy equation describing this heat transfer process is given by:

$$\rho C_p \frac{DT}{Dt} = k\nabla^2 T \qquad (2)$$

where ρ is the density of air, C_p is the specific heat of air, k is the thermal conductivity of air, and T the air temperature. The effect of convection on the heat transfer process is taken into account in the derivative term DT/Dt of Eq. 2:

$$\frac{DT}{Dt} = \frac{\partial T}{\partial t} + V.grad(T) \tag{3}$$

where V is the velocity field in the air. The steady state case was solved, such as the time derivative term $\partial T/\partial t$ in Eq. 3 is set to zero. A condition of continuity of heat flow has been taken for the upper edges and the external face of the cones.

The temperature of the condenser will be lower than that of the ambient air due to the radiative cooling. Natural convection will thus appear, enhancing heat transfer between air and condenser. This effect can be taken into account by a temperature dependence of the fluid density (buoyancy effect) in the conservation of momentum equation. However, the coupling forced-natural convection is difficult to account (it needs a long iterative process) and the effect of convection, which matters only for weak air flow velocity is neglected in this study.

In the solid domain, conduction is modeled using a simple heat equation. No-slip boundary condition is for all condenser surfaces. The Reynolds number, which compares the inertial forces with the viscous forces and determines whether the flow is turbulent or laminar, reads as

$$\mathrm{Re} = \frac{VL}{\nu} \tag{4}$$

Here $L \approx 10$ m is the condenser typical lengthscale; ν is air kinematic viscosity and V is wind speed, giving $\mathrm{Re} \approx 7\times 10^5\ V$. Laminar flow is expected for a Reynolds number lower than a critical value, which depends on the geometry. It is on order of 2000 for cylinders but can be reduced depending on the geometry. As a matter of fact, turbulence was observed even for wind speed as low as 10^{-4} m.s^{-1}.

The Navier Stockes equations are solved with the $k-\varepsilon$ turbulence module because it performs quite well for external flow problems around complex geometries.

After some trials, it was considered for the simulation a box of 75 m long, 20 m wide and 8 m high whose top is at 8m above the lower part of the cones, in accord with the specifications noted in Section 2.2. The large value of the box length is necessary because the effects of pressure matter and were seen on smaller boxes.

All of the meshes created in COMSOL Multiphysics were physics controlled and automatically generated. The meshes varied in size ranging from a coarser mesh all the way up to a normal mesh. Several mesh sensitivity tests were carried out to demonstrate the dependency of the results on various types of meshes. No relevant differences have been identified in the velocity field of the upstream and downstream flow and in the temperature field.

The final aim of the CFD numerical is to estimate the dew water output with respect to the meteorological parameters. This is a very general and difficult task and up to now several simplifications have been made to retain only the most important parameters. As the actual yield per surface area, h, depends on the supersaturation reached by the condensing substrate, the determination of the temperature drop (T_a-T_c) (T_c is the condenser surface temperature) with respect to air temperature can represent the dew yield as shown in Appendix 1. Total yield is calculated from h and the condensing surface area, S_c (=hS_c).

3. Results and discussion

3.1. Air flow

The two S- and W-shapes have been tested with the Ansys CFX simulation with incoming air velocity 0.5, 1, 2, 3, 4, 5 m.s^{-1} at 10 m elevation. The main result is that, while the inside air flows are different for S-and W-shapes, the variation of wind speed does not appreciably affect the aerodynamic performances of the two cones. One thus only report data in Figs. 3 and 4 corresponding to the wind speed values 0.5 and 2 m.s^{-1}.

277 Figures 4abcd compares the aerodynamic effects on a symmetry plane along the wind direction for S-
278 and W- cones for wind speed values 0.5 and 2 m.s^{-1}. Increasing the wind speed only reinforces the fact
279 that lower wind speed is seen in the S-cone central air volume than in the W-cone. In addition, above
280 the cones, higher streamline development above the W-cone signs a more turbulent airflow than above
281 the S-cone.

282

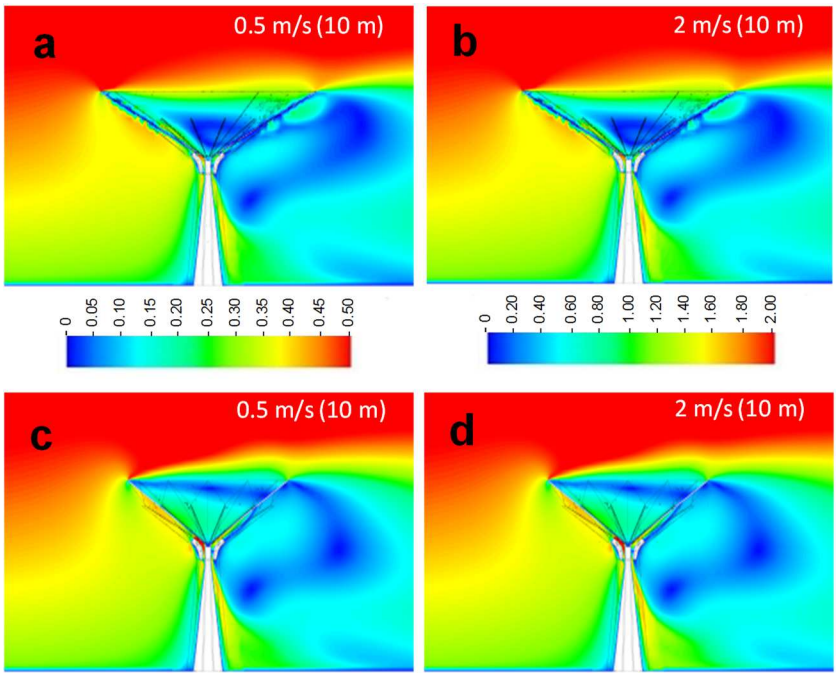

283

284 Fig. 3. Air flow (from left to right) at two different incoming velocities on vertical sections at the cone axes, on the symmetry
285 plane along the wind direction. (a,b): S-cone. (c,d): W-cone. Air flow is from left to right.

286 Figures 4abcd visualize the wind velocity on the internal surface of the condenser, which is of prime
287 importance for convective heat transfer. Increasing the incoming wind velocity changes has very little
288 effect. In contrast, wind on S-cone internal surface is seen to be lower than on the W-cone surface.

289

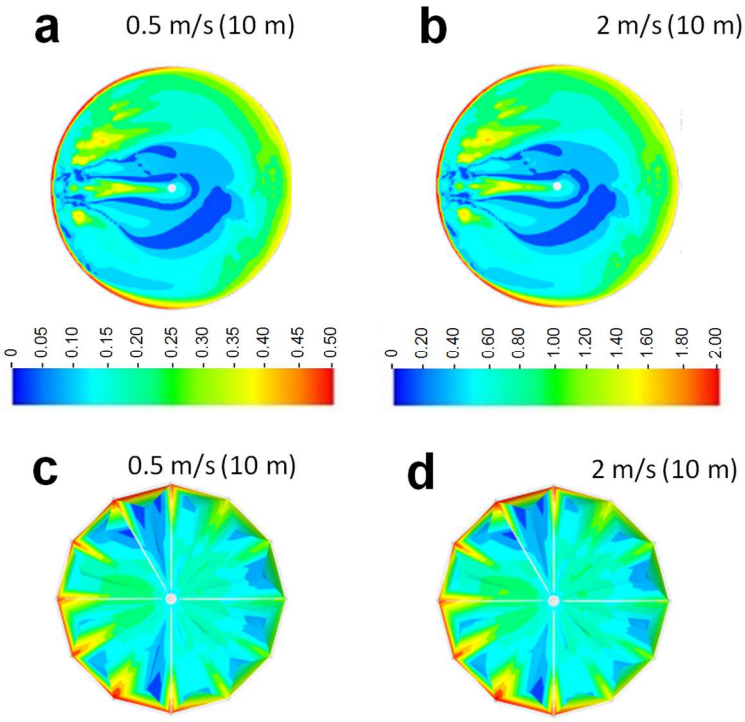

Fig. 4. Air flow (from left to right) at two different incoming velocities on vertical sections at the cone axes, on the symmetry plane along the wind direction. (a-b): S-cone. (c-d): W-cone. Air flow is from left to right.

One thus sees that condenser' surface velocity is largely affected by external and internal geometry. Smoother geometries help to maintain low wind speed at condenser' surface. Velocity at condenser' surface is higher in the W-cone than in the S-cone as caused by the triangulated external surfaces and exposed highest edges of the condenser. One thus expects enhanced convective heat transfer with the W-cone.

Some studies have been carried out with COMSOL at two typical wind speeds at 10 m elevation, a very low speed of 10^{-4} m.s^{-1} where the Reynolds number Re ≈ 70 and a speed of 2 m.s^{-1} (Re ≈ 1.4×10^{6}). The latter value is a mean value for dew formation (which in average occurs between 0 and 4.4 m.s^{-1}, see Beysens, 2018) and corresponds to the mean wind speed during night at the site where such condensers should be implemented. The low speed value (10^{-4} m.s^{-1}) was chosen because the simulation with CFX, which was looking for variations in aerodynamic patterns, did not find significant differences between high and low wind speed. The aerodynamics of the design performs

similarly at all wind conditions tested. Then the decision of modeling the wind at 10^{-4} m.s^{-1} has been taken as this represents a "little to no-wind" scenario that is likely to be experienced on site. In addition, this low wind condition helps to reach convergent solutions in a reasonably short time span by reducing turbulent effects. Although turbulence is seen even at low wind speed (Fig. 5), stagnation of the flow is also observed, which limits the convective heat exchanges and facilitates dew formation.

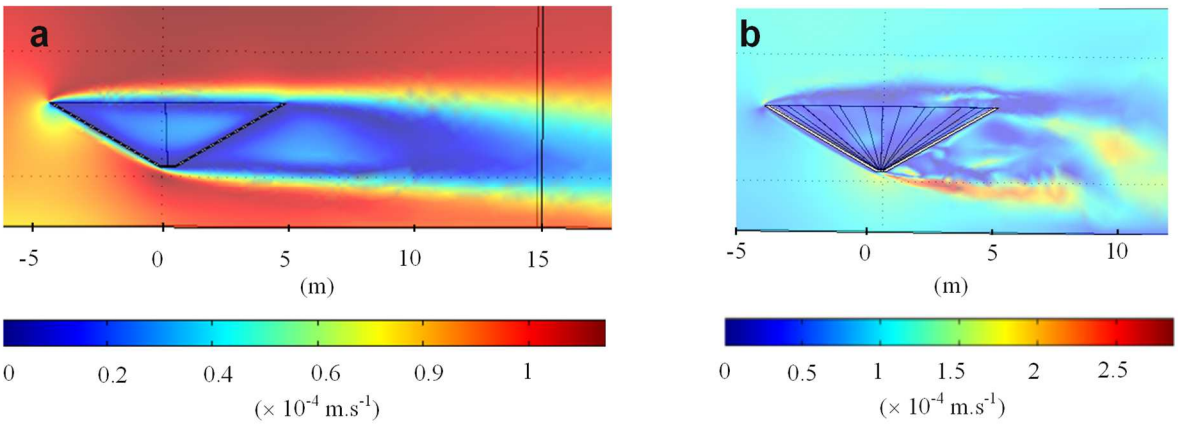

Fig. 5. Turbulence observed at low wind speed 10^{-4} m.s^{-1} for (a) S-cone and (b) W-cone. Air flow is from left to right.

3.2. Surface temperature

Temperature of the inner surface of the cones are reported in Figs. 6abcd for both W- and S-cones at the two wind speeds of 10^{-4} m.s^{-1} and 2 m.s^{-1} and summarized in Table 2. For 10^{-4} m.s^{-1} windspeed, the mean cooling with respect to air temperature is found to be 5.85 K (S-cone) and 6.55 K (W-cone), and for 2 m/s windspeed, 5.49 K (S-cone) and 5.25 K (W-cone). Corrugation increases on one hand radiative cooling but on the other hand reduces cooling by enhanced convective heat exchange. At low speed, convective heat exchange is similar for both smooth and corrugated surfaces, and corrugation increases cooling for the W-cone. At higher air flow velocities, convective heat exchange is larger for the W-cone and cooling is eventually found smaller than for the smooth cone. However, the difference (0.24 K) remains small. Details of air temperature are also shown in Fig. 6ef. Air is seen to cool down after having passed near the cone edge.

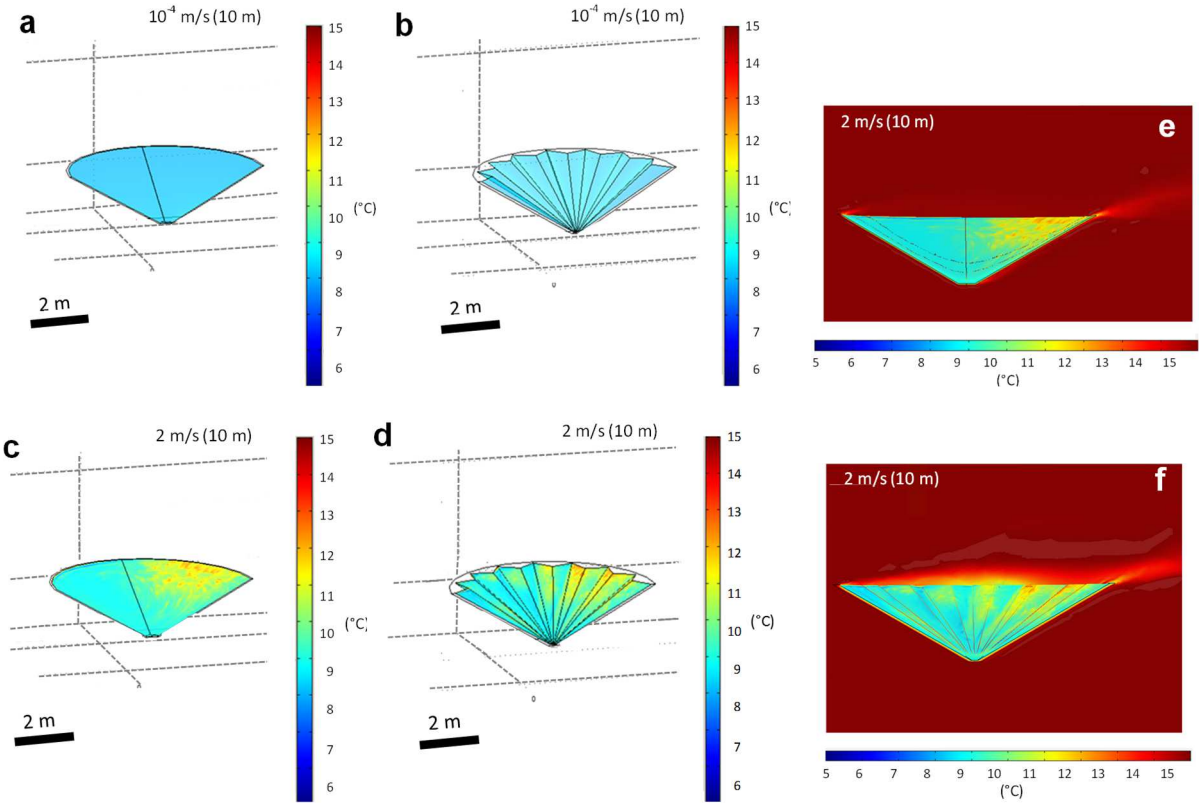

Fig. 6. (a-d): Surface temperatures of S- cone and W-cones. Air flow is from left to right. (a,b): Windspeed 10^{-4} m.s^{-1}. (c,d): Windspeed 2 m.s^{-1}. Air temperature is shown in (e,f). Significant cooling with respect to the initial temperature of 15°C is observed.

	V (m.s^{-1})	$\langle T_c \rangle$ (°C)	$\langle T_c \rangle - T_a$ (°C)
S-cone	10^{-4}	9.15	5.85
	2	9.51	5.49
W-cone	10^{-4}	8.45	6.55
	2	9.75	5.25

Table 2. Results of the simulation at two different wind speed V showing the mean surface temperature $\langle T_c \rangle$ and mean cooling temperature $\langle T_c \rangle - T_a$ with respect to air temperature T_a = 15°C.

4. Conclusion

From a detailed analysis of air flows around corrugated W-cone and smooth S-cone, it appears clearly that, although the inside air flows are different for the two shapes, the variation of wind speed does not

appreciably affect the aerodynamic performances of the two cones. The scooping effect however performs better in the S-shape than in the W-shape, with wind speed on the internal surface of the S-cone lower compared to the W-shape. The shape of the crown in the S-shape cone indeed amplifies the upward trajectory of the wind that is redirected away from the inner area of the cone as it hits the edge of attack; this geometrical feature helps significantly in reducing the wind speed on the internal surface of the S-cone compared to the W-shape.

From these air flow characteristics, it naturally follows that the W-cone, which radiates more, also cools more at low windspeed than the S-cone where the convective heat transfer is low. In contrast, at large windspeed, the W-cone cools less as an effect of enhanced convective heat transfer in the corrugated structure. For typical air flow velocity of 2 $m.s^{-1}$, the difference in mean cooling between both shapes remains, however, small (0.24 K). Since cooling temperatures are nearly proportional to dew yield for the weak cooling temperatures as encountered in dew condensation, it means that the corrugated W-cone, which exhibit better dew drop collecting properties, will give a final better dew collection yield per surface area than the corresponding smooth S-cone. Total yield will obviously has to account for the different W and S cone actual surface areas. In the example reported here with 24 faces for the W-cone, the S-cone exhibits a surface larger than the W-cone.

References

Agam, N., Berliner, P.R., 2006. Dew formation and water vapor adsorption in semi-arid environments—a review. J. Arid. Environ. 65, 572–590.

Beysens, D., 2018. Dew water (Rivers Publisher, Gistrup).

Beysens, D., Broggini, F., Milimouk-Melnytchouk, I., Ouazzani, J., Tixier, N., 2013. New architectural forms to enhance dew collection. Chemical Engineering Transactions 34, 79-84.

Bliss R.A., 1961. Atmospheric radiation near the surface of the ground. Solar Energy 5, 103-20.

Blocken, B., Stathopoulos, T., Carmeliet, J., 2006. CFD simulation of the atmospheric boundary layer: wall function problems. Atmospheric Environment 41, 238-252.

Clus, O., Ouazzani, J., Muselli, M., Nikolayev ,V. S., Sharan, G. Beysens, D., 2009. Comparison of various radiation-cooled dew condensers using computational fluid dynamics. Desalination 249, 707-712.

Kaseke, K., Wang, L., Seely, M., 2017. Non-rainfall water origins and formation mechanisms. Science Advances 3, e1603131.

Kaseke, K., Wang, L., 2018. Fog and dew as potable water resources - maximizing harvesting potential and water quality concerns. GeoHealth 2, 327-332.

Liu, M., Cen, Y., Wang, C., Gu, X., Bowler, P., Wu, D., Zhang, L., Jiang, G., Beysens, D., 2020. Foliar uptake of dew in the sandy ecosystem of the Mongolia Plateau: A life-sustaining and carbon accumulation strategy shared differently by C3 and C4 grasses. Agricultural and Forest Meteorology 287, 107941.

Medici, M.-G., Mongruel, A., Royon, L., Beysens, D., 2014. Edge effects on water droplet condensation, Phys. Rev. E 90, 062403.

Mochida, A., Tominaga, Y., Yoshie, R., 2006. AIJ guideline for practical applications of CFD to wind environment around buildings. The 4th International Symposium on Computational Wind Engineering (CWE2006, Yokohama) 533-536.

Pal Arya, S., 1988. Introduction to Micrometeorology (Academic Press, Inc., San Diego).

Tomaszkiewicz, M., Abou Najm, M., Beysens, D., Alameddine, I., El-Fadel, M., 2015. Dew as a sustainable non-conventional water resource: a critical review. Environmental Reviews, 23, 425-442.

Appendix 1

This calculation reproduces the main features of the model developed in Beysens (2018). When considering an energy balance equation it is possible to elaborate a relation between surface temperature without condensation, under dry air, and dew yield obtained with humid air at same temperature.

Let us consider a condenser surface thermally isolated from below of surface area S_c. For condenser mass dM around a point of coordinate (x, y, z) with condensing surface area dS_c, the energy balance reads as:

$$\frac{dT_c}{dt}(dMC_c + dmC_w) = R_i dS_c + R_{he} + R_{cond} \quad \text{(A1)}$$

Here T_c is the surface temperature of the condenser, dm is the mass of water condensate, C_c and C_w are the specific heats of the condenser materials and water, respectively. Without condensation $R_{cond} = 0$ and at equilibrium $dT_c/dt = 0$, the condenser surface temperature reaches T_{c0} under radiative cooling $R_i(x,y,z)$ balanced by convective heat losses $R_{he}=a(x,y,z)\,(T_a-T_{c0})$. The latter us Newton law with a the convective heat transfer coefficient. With T_a the air temperature, Eq. A1 becomes:

$$0 = R_i(x,y,z) - a\left[T_a - T_{c0}(x,y,z)\right] \quad \text{(A2)}$$

It follows the determination of the local convective heat transfer coefficient $a(x,y,z)$:

$$a(x,y,z) = \frac{R_i(x,y,z)}{[T_a - T_{c0}(x,y,z)]} \quad \text{(A3)}$$

Let us now consider dew condensation. The condensation rate is $R_{cond} = L_c\dot{m}$ where $\dot{m} = dm/dt$. At thermal equilibrium $dT_c/dt=0$, it follows from Eq. A1 for the dew yield per unit surface:

$$\frac{d\dot{m}}{dS_c} = \frac{R_i(x,y,z)}{L_c}\left[1 - \frac{T_a - T_c}{T_a - T_{c0}(x,y,z)}\right] \quad \text{(A4)}$$

Making the simplification $T_c \approx T_d$, with ϱ_w the liquid water density, the dew yield per unit surface area can be written as

$$\dot{h} = \frac{1}{\varrho_w}\frac{d\dot{m}}{dS_c} \approx \frac{R_i(x,y,z)}{\varrho_w L_c}\left[1 - \frac{T_a - T_d}{T_a - T_{c0}(x,y,z)}\right] \quad \text{(A5)}$$

Defining the mean value of variable $Q(x,y,z)$ on surface S_c by

$$\langle Q \rangle = \frac{1}{S_c}\int_{S_c} dS_c \,, \quad \text{(A6)}$$

equation A5 can be rewritten as

$$\langle \dot{h} \rangle = \frac{1}{\varrho_w L_c}\left[\langle R_i(x,y,z)\rangle - (T_a - T_d)\left\langle \frac{R_i(x,y,z)}{T_a - T_{c0}(x,y,z)}\right\rangle\right] \quad \text{(A7)}$$

Depending on the shape of the condenser, approximations can be made to relate $\langle \dot{h} \rangle$ to $\langle R_i \rangle$ and $\langle T_a - T_{c0} \rangle$. Either R_i is a weak function of (x,y,z),

$$\langle \dot{h} \rangle = \frac{R_i}{\varrho_w L_c}\left[1 - \frac{(T_a - T_d)}{T_a - \langle T_{c0}(x,y,z)\rangle}\right], \quad \text{(A8)}$$

or T_{c0} is a weak function of (x,y,z):

$$\langle \dot{h} \rangle = \frac{\langle R_i(x,y,z)\rangle}{\varrho_w L_c}\left[1 - \frac{(T_a - T_d)}{T_a - T_{c0}}\right] \quad \text{(A9)}$$

Both Eqs. A8 and A9 can be rewritten as

$$\langle \dot{h} \rangle = \frac{\langle R_i \rangle}{\varrho_w L_c} F_{a,d}(T_{c0}) \quad \text{(A10)}$$

where the function $F_{a,d}(T_{c0})$ is

$$F_{a,d}(T_{c0}) = 1 - \frac{T_a - T_d}{T_a - \langle T_{c0} \rangle} \quad \text{(A11)}$$

Figure A1 represents the variations of $F_{a,d} = 1 - 3.4/(T_a - \langle T_{c0} \rangle)$ as a function of $T_a - \langle T_{c0} \rangle$ corresponding to the current nightly conditions T_a = 288.15 K (15 °C), RH = 80%, with dew point temperature T_d=11.6°C and T_a-T_d=3.4°C. Data have been drawn only for positive $\dot{h}$ values, that is for $T_a - \langle T_{c0} \rangle$ > 3.4°C, and a temperature cooling range that does not exceeds the maximum value 10°C. In this range [3.4°C-10°C], the variation of F can be approximated by the linear relationship

$$F_{a,d} \approx A(T_a - \langle T_{c0} \rangle) \quad \text{(A12)}$$

This linear relationship thus means that the dew yield $\dot{h}$ is approximately proportional to the temperature cooling $(T_a - \langle T_{c0} \rangle)$. Such a proportionality has indeed been observed by Clus et al. (2009) when comparing measured dew yields and temperature drop determined by CFD.

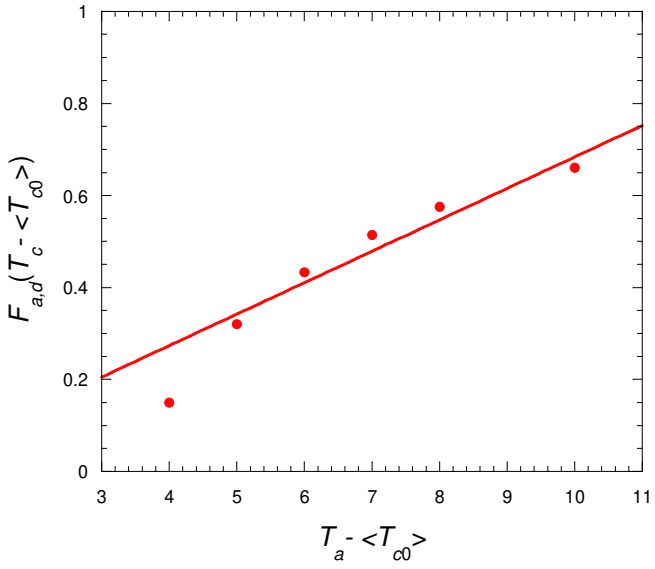

Fig. A1. Variations of $F_{a,d}$ as a function of $T_a - \langle T_{c0} \rangle$ according to Eq. A11 for typical night conditions T_a = 288.15 K (15°C), RH = 80%, corresponding to T_a-T_d = 3.4°C, in the range [3.4°C-10°C] (see text). The line is a fit to Eq. A12 with A = 0.068 ± 0.003 and a correlation coefficient R = 0.95.